Influence of Nanostructure Geometry on Electronic Properties

2014 IOP Conf. Ser.: Mater. Sci. Eng. 60 012055

(http://iopscience.iop.org/1757-899X/60/1/012055)

Influence of Nanostructure Geometry on Electronic Properties

A Tavkhelidze
Ilia State University, Cholokashvili Ave. 3-5, Tbilisi 0162, Georgia

E-mail: avtotav@gmail.com

Abstract. Recently, new quantum features have been studied in the area of nanostructured layers. It emerges that properties of nanostructures depend not only on their size but also on their geometry. Particularly, a nanograting (NG) on the surface of the thin layer imposes additional boundary conditions on electron wave function and forbids some quantum states. Density of quantum states reduces. Unlike conventional quantum well, state density per volume, is reduced in the case of NG layer. This leads to changes in electronic properties. Electrons, rejected from forbidden quantum states, have to occupy states with higher energy. In the case of semiconductor layers, electrons rejected from the valence band have to occupy empty quantum states in the conduction band. Such increase in conduction band electron concentration can be termed as geometry-induced doping or G-doping. G-doping is equivalent to donor doping from the point of view of the increase in electron concentration. However, there are no ionized impurities. This preserves charge carrier scattering to the intrinsic semiconductor level and increases carrier mobility with respect to the donor-doped layer. As rejected electrons occupy quantum states with the higher energy, the chemical potential of NG layer increases and becomes NG size dependent. We regard a system composed of NG layer and an additional layer on the top of the NG forming periodic series of p–n junctions. In such system, charge depletion region develops inside the top of NG and its effective height reduces, becoming a rather strong function of temperature *T*. Consequently, *T*-dependence of chemical potential magnifies and Seebeck coefficient *S* increases. Calculations show one order of magnitude increase in the thermoelectric figure of merit *ZT* relative to bulk material. In the case of metal layers, electrons rejected from forbidden quantum states below Fermi energy, occupy quantum states above Fermi energy. Fermi energy moves up on energy scale and work function (WF) reduces. WF reduction was observed in thin amorphous Au films grown on thermally oxidized Si substrates. WF was measured using Kelvin Probe and PEEM microscope. WF reduction depended on film internal structure and NG sizes. Maximum reduction in WF of 0.56 eV has been obtained.

1. Introduction

Developments in nanotechnology allow fabrication of densely packed, periodic structures [1-4]. Recently, ultra-short period nanopore arrays and nanogratings have been obtained by block copolymer lithography [1, 2]. Another method for nanograting (NG) fabrication is a multi-beam interference lithography. Using these techniques, gratings with 10-nm [3] and even sub-10 nm pitch [4] were fabricated. At the same time, it has been shown that NG dramatically improves thermoelectric [5] and electron emission properties [6] when grating pitch becomes comparable with electron de Broglie wavelength. This is owing to special boundary conditions imposed by NG on electron wave function. Supplementary boundary conditions forbid some quantum states, and density of quantum states (DOS)

reduces (in all bands). Electrons rejected from NG-forbidden quantum states have to occupy empty states with a higher energy. Fermi energy increases and electronic properties of NG layer change.

Qualitatively, DOS reduction can be described by the de Broglie wave reflection. Let us regard a solid/vacuum interface with NG on the surface (figure 1).

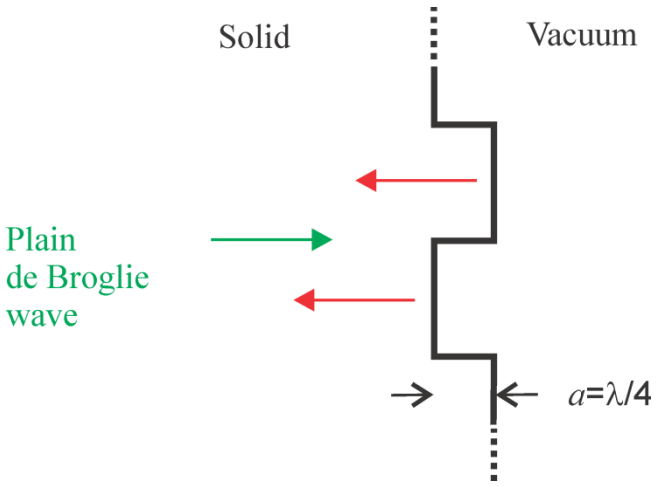

Figure 1. Reflection of plane de Broglie wave from the NG surface.

Let us consider an electron with energy $E < E_F$ (where E_F is Fermi energy), moving towards the border of the solid as a planar de Broglie wave. It will reflect back from the interface as the electron does not have enough energy to leave the solid. There will be two reflected waves. One reflected from the top of the indent and another from the bottom of the indent. If the indentation depth $a = \lambda / 4$, where λ is electron de Broglie wavelength, two reflected waves will interfere destructively resulting in no reflected wave. Consequently, an electron of certain energy cannot reflect back from the surface. On the other hand, the electron cannot leave solid to vacuum as it does not have enough energy to overcome the potential barrier ($E < E_F$). It cannot reflect under arbitrary angle as it is in the Fermi gas in which all quantum states are already occupied. Therefore, all possible final quantum states for that particular electron are forbidden. As all the final states are forbidden, the initial state with wave vector $k = \pi / 2a$ is also forbidden. Obviously, all states with wave vector component $k_Z = (\pi / a)(p + 1/2)$, where p is integer are also forbidden. As a result, DOS near the interface is reduced with respect to the plain solid.

Qualitative description of DOS reduction is demanding. The calculation requires solving of the time-independent Schrödinger equation in the NG geometry. Mathematically, there is no difference between DOS reduction and the electromagnetic (TM) mode depression [7, 8]. Helmholtz equation and Dirichlet boundary conditions are used in both cases. Unfortunately, there is no exact analytical solution for NG geometry. The approximate analytical expression known as Weyl's formula [9, 10] allows calculation of DOS using a ratio of layer surface and volume. Perturbation method [11] has been used to find an approximate analytical expression for *G* in NG geometry. DOS for electromagnetic modes in resembling geometries has been numerically calculated in the literature related to the Casimir effect [12].

Influence of periodic structures on electronic properties has been studied in related geometries such as periodic curved surfaces [13, 14], nanotubes [15], cylindrical surfaces with non-constant diameter [16] and strain-driven nanostructures [17].

2. Semiconductor nanograting layers

In the case of semiconductor materials, electrons rejected from the valence band (VB) occupy empty quantum states in the conduction band (CB). Electron concentration *n* in the CB increases which can be termed as geometry-induced electron doping or G-doping. G-doping is equivalent to donor doping from the point of view of increase in n and Fermi energy. However, there are no ionized impurities. This maintains charge carrier scattering to intrinsic semiconductor level and increases carrier mobility with respect to the donor-doped layer of same electron concentration. G-doping is temperature independent as it originates from layer geometry and no ionized impurities are involved.

Other methods of doping without impurities are well known modulation doping and recently introduced polarization doping [18]. Both are 2D in their nature. However, a 3D approach of modulation doping was introduced in [19] to improve thermoelelectric characteristics of nanocomposites [20].

Electron confinement to the NG layer is needed to obtain G-doping. The layer can be made free standing but in practice it is usually sandwiched between wide band gap layers. NG layer thickness is fundamentally limited by the requirement of having quantum properties. However, thin layers have low optical absorption. Layer thickness also limits lateral charge and heat transport.

Figure 2 shows a cross section of a single NG layer. The grating has depth a and period $2w$. To make a comparison, we choose reference layer as plain layer with thickness H such that it has the same cross section area.

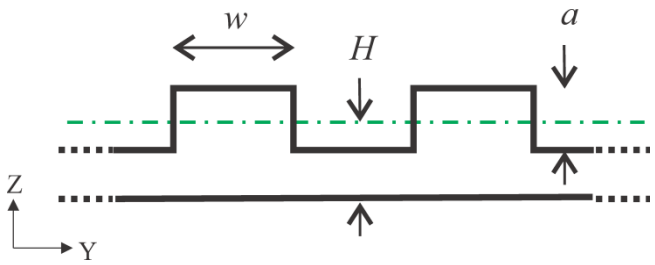

Figure 2. Cross section of nanograting layer.

Nanograting imposes additional boundary conditions on electron wave function and forbids some quantum states. The DOS in energy $\rho(E)$ reduces [21] with respect to the reference well

$$\rho(E) = \rho_0(E)/G. \qquad (1)$$

Where $\rho_0(E)$ is the DOS (number of quantum states within the unit energy region and in the unit volume) in a reference well and $G = G(H, w, a) > 1$ is the geometry factor. With increasing NG depth DOS reduces.

Nanograting reduces DOS in all bands. Electrons rejected from the NG-forbidden quantum states have to occupy empty quantum states with higher E. In a semiconductor, electrons rejected from the VB have to occupy empty (and not forbidden by NG) energy levels in CB (figure 3). Electrons reject from low energy levels and occupy high energy ones. During this process, Fermi energy increases from $E_F^{(0)}$ to E_F. To simplify the presentation, in figure 3, we presume that T=0 (T is absolute temperature) and energy levels are equidistant on the energy scale (geometry-induced energy level shift is also ignored).

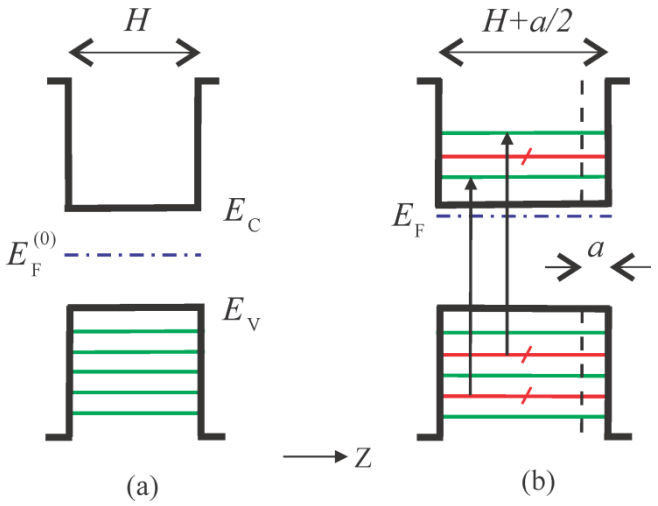

Figure 3. Energy diagrams of a) reference semiconductor quantum well and b) NG layer. Green lines depict occupied energy levels. Red lines depict NG-forbidden energy levels.

We will employ (1) to calculate the DOS and investigate G-dependence of n and E_F. The density of the NG-forbidden quantum states is

$$\rho_{\mathrm{F}}(E) = \rho_0(E) - \rho_0(E)/G = \rho_0(E)(1-1/G). \qquad (2)$$

To determine the number of rejected electrons n_r (per unit volume), (2) should be integrated over the electron confinement energy region.

$$n_{\mathrm{r}} = \int_{\mathrm{con}} dE\, \rho_{\mathrm{F}}(E) = (1-1/G) \int_{\mathrm{con}} dE\, \rho_0(E) = (1-1/G)\, n_{\mathrm{con}}. \qquad (3)$$

Where, $n_{\mathrm{con}} = \int_{\mathrm{con}} dE\, \rho_0(E)$. n_{r} Here, we assume that electron confinement takes place only in narrow energy intervals inside which G is energy-independent. In most cases, thin layer is grown on a semiconductor substrate and confinement energy regions are band offsets.

There are distinctions and similarities between the NG forbidden quantum state and a hole. The state is forbidden by the boundary conditions and cannot be occupied. However, it is not forbidden in an irreversible way. If the boundary conditions change (e.g., owing to charge depletion), then it can recombine with the electron (like the hole recombines with the electron). As the NG forbidden state is confined to the boundary conditions (macroscopic geometry), it is not localized in the lattice and cannot move like a hole.

3. Electronic properties of multiple homojunction nanograting layer

To obtain electron confinement in multiple NG layers transitional barrier layers are required. We regard cases of wide band gap material forming homojunction. Confinement regions originate from barrier layer donor doping.

Here, we investigate G-doping in multiple NG layers. Such layers are quasi-3D and have improved optoelectronic and thermoelectric characteristics with respect to a single layer. Multiple NG layers consist of a replicated structure including main and barrier layers forming a series of hetero or homo junctions. Main layer is thicker than a barrier layer and plays a leading role in carrier transport and

optical absorption. Barrier layer forms electron confinement energy regions. It also contributes to carrier transport and optical absorption. Both main and barrier layers have NG geometry.

One of the objectives of this work is to calculate n and in multiple NG layers and find out how they depend on layer thicknesses and material properties. First, we introduce G-doping in a single NG layer. Next, we calculate n and in a homojunction multilayer structure. Subsequently, we calculate the same for a heterojunction multilayer structure. Finally, the possibility of realization of such structures and their advantages for optoelectronic and thermo-electric devices are discussed. An analysis was made within the limits of parabolic band, wide quantum well and degenerate electron gas approximations.

We begin from calculating *n* in a homojunction NG layer, as it is relatively straightforward. Homojunction is formed between intrinsic main layer and donor-doped barrier layer. Let us consider a case when all layers have a plain geometry (NG is not formed yet). Figure 4a shows an energy diagram of such structure (typically obtained by homoepitaxal growth) [22]. Charge depletion regions form inside the both i-type main layer and n-type barrier layer. Band edges curve, shaping confinement regions in the main layer VB and in the barrier layer CB. Electrons with energies $E_V - \Delta E_{con}^{(0)} < E < E_V$ are confined to main layers and ones with energies $E_C - \Delta E_{con}^{(0)} < E < E_C$ are confined to barrier layers. Here, we assume that both main and barrier layers are relatively thick so that electron wave functions do not overlap and we can ignore the mini band formation.

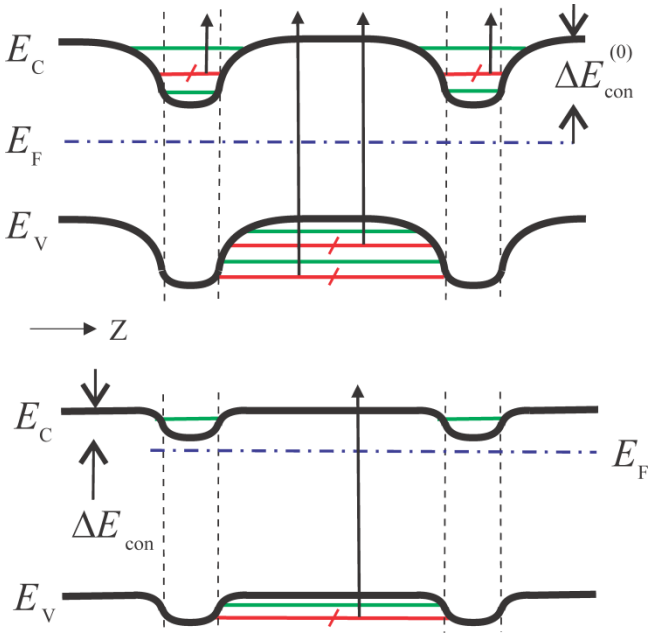

Figure 4. Homojunction structure energy diagrams: a) before NG formation, b) after NG formation. Green lines depict occupied energy levels. Red lines depict NG-forbidden energy levels.

3.1. Influence of Nanograting

Next, we fabricate NG on the surface of all layers simultaneously (fabrication of such structure will be discussed later in this work). Nanograting forbids some energy levels (red lines) and induces G-doping depending on geometry factor value. We introduce two geometry factors G_m and G_b for the main and barrier layers separately (layers have different geometry factors owing to a different thickness).

If $G_m > 1$ some electrons reject from the VB of main layer (figure 4). If $G_b > 1$ some electrons reject from the CB of barrier layer and occupy higher energy levels in the same band. In the beginning,

let us regard the case $G_m > 1 \text{ and } G_b = 1$. As $G_m > 1$, the Fermi level increases in main layer, which is equivalent to shifting band edges down on the energy scale. As $G_b = 1$, the bang edges remain intact in barrier layer. With the downward shift in main layer, VB confinement region will shrink and fewer electrons will reject to the CB. This will continue until some equilibrium value of rejected electrons is achieved. In other words, band edge downward shift provides negative feedback to the G-doping process. Next, let us regard the case $G_m > 1 \text{ and } G_b > 1$. Here, barrier layer band edges also shift down. Owing to the downward shift in barrier layer, confinement energy regions widen. This increases the number of rejected electrons in main layer. In other words, barrier layer G-doping provides positive feedback to main layer G-doping. Finally, we have a combination of negative feedback originating from main layer and positive feedback origination from barrier layer. In the case of overall negative feedback G-doping of two layers will saturate and equilibrium value of ΔE_{con} will be attained (figure 4b). Last depends on G_m, G_b and semiconductor material parameters.

3.2. Electron confinement energy region

To find ΔE_{con} we have to calculate electron concentrations in both main and barrier layers first. Applying (2) to the main layer we find the number of rejected electrons

$$n_r = (1-1/G_m) \int_{E_V}^{E_V - \Delta E_{con}} dE\, \rho_{0V}(E) \qquad (4)$$

where, $\rho_{0V}(E)$ is the initial (to NG) DOS in the main layer VB. Let us regard the case when the rejected electron number is much more than the initial electron number in CB $n_r >> n_0$. Then, the CB electron concentration will be merely n_r. Further, we use the following well known expression for valence band DOS to calculate n_r [23]

$$\rho_{0V}(E) = 2\pi^{-1/2} N_V (k_B T)^{-3/2} (E - E_V)^{1/2} \qquad (5)$$

Here, N_V is the effective VB density of states. Inserting (5) in (4) and integrating, choosing zero of energy scale as $E_V = 0$ we find

$$n_r = (4/3\sqrt{\pi})\, N_V (1-1/G_m)(\Delta E_{con}/k_b T)^{3/2} \qquad (6)$$

Further, we find Fermi levels in both layers using corresponding electron concentrations. According to the well known expression for degenerate semiconductor [24] Fermi level in main layer can be found from

$$E_F - E_C^{(m)} = k_B T \left[\ln (n_r / N_C) + 2^{-3/2} (n_r / N_C)\right] \qquad (7)$$

where, N_C is the effective CB density of states. CB electron concentration of barrier layer does not change during NG formation, as there are no electrons transferred from the VB to the CB. However, Fermi level in the barrier layer moves up on an energy scale owing to NG-induced reduction in N_C

$$E_F - E_C^{(b)} = k_B T\left[\ln\left(G_b\, n_d / N_C\right) + 2^{-3/2}\left(G_b\, n_d / N_C\right)\right] \qquad (8)$$

Here, n_d is barrier layer initial electron concentration (obtained by donor doping). Energy diagram (figure 4) shows that $\Delta E_{con} = E_C^{(m)} - E_C^{(b)}$. Subtracting (7) from (8) and inserting in the last expression we find

$$\left(\Delta E_{con} / k_B T\right) = \ln\left(G_b\, n_d / n_r\right) + 2^{-3/2}\left[\left(G_b\, n_d - n_r\right) / N_C\right]. \qquad (9)$$

Inserting (6) in (9) and depicting $\eta \equiv \Delta E_{con} / k_B T$ we get following nonlinear equation for η

$$\eta + \frac{3}{2}\ln\eta + 2^{-3/2}\,\frac{4}{3\sqrt{\pi}}\,\frac{N_V}{N_C}\,\frac{G_m - 1}{G_m}\,\eta^{3/2} - \ln\frac{3\sqrt{\pi}\,G_m G_b\, n_d}{4N_V\left(G_m - 1\right)} - 2^{-3/2}\,\frac{G_b\, n_d}{N_C} = 0 \qquad (10)$$

Equation (10) was solved numerically to find ΔE_{con} using two geometry factor and n_d, N_C, N_V values for Si and GaAs materials.

3.3. Electron concentration and Fermi level

Numerical solutions of (10) were inserted in (6) to find n_r. Next, we found the Fermi level of the main layer by inserting values of n_r in (7). Formula (8) was used to find a Fermi level position in barrier layer. Table 1 shows the results for geometry factors G_m=1. 02, $G_b = 1.1$ and *T*=300 K.

Table 1. Electron concentration and Fermi levels in main and barrier layers for Si and GaAs materials. Energy was measured from corresponding layer CB edge.

Material	n_d [cm^{-3}]	ΔE_{con} [meV]	n_r [cm^{-3}]	$E_F^{(m)}$ [meV]	$E_F^{(b)}$ [meV]
Si	3 x 10^{18}	45	6 x 10^{17}	103	58
	1 x 10^{19}	64	1 x 10^{18}	89	25
	3 x 10^{19}	87	1 x 10^{18}	77	-10
	1 x 10^{20}	126	2.8 x 10^{18}	62	-64
GaAs	1 x 10^{18}	47	3.2 x 10^{17}	3.4	-44
	3 x 10^{18}	86	8 x 10^{17}	-29	-115
	5 x 10^{18}	119	1.3 x 10^{18}	-52	-172
	1 x 10^{19}	197	2.8 x 10^{18}	-110	-297

For barrier donor doping levels 10^{18}-10^{20} cm^{-3} and G values rather close to unity (G_m=1.02, $G_b = 1.1$) main layer G-doping levels of 10^{17}-10^{18} cm^{-3} were obtained. We chose this range of G-dropping levels, as they are frequently used in applications. Higher and lower G-doping levels can be obtained as well. Table 1 shows that one order higher donor doping n_d (10^{20} cm^{-3}) is needed in Si with respect to GaAs (10^{19} cm^{-3}) to obtain a G-doping level 2.8 10^{18} cm^{-3}. It is convenient to give an interpretation of this result using terms of negative and positive feedback. Negative feedback in main layer is weaker for Si material as it has higher n_0 value with respect to GaAs. Owing to the high value of n_0, band edges shift down less rapidly with increasing n_r, following well known logarithmic dependence

$\Delta E_F = k_B T \ln(n_r / n_0)$. As ΔE_F is positive in our case, higher n_0 results in weaker negative feedback. Weaker negative feedback in the main layer requires weaker positive feedback in the barrier layer to obtain equilibrium. Positive feedback is weaker in highly donor-doped barrier layers (as shifting band edges require more rejected electrons). This explains why higher n_d is required in Si barrier layer with respect to GaAs.

As figure 4 shows there are potential barriers for electrons in the CB and holes in the VB of multilayer NG. They are affecting carrier transport in Z direction. However, barrier height is ΔE_{con} which is of the order of a few $k_B T$ as table 1 indicates (except for very high level of donor doping. $k_B T$ =26 meV for *T*=300 K). Charge carriers easily overcome such obstacles (thermionic emission) and their influence can be ignored. In the case of high values of ΔE_{con} barriers may block carrier transport in Z direction. To avoid this, high level of G-doping should be obtained not by increasing donor doping of barrier layers but by increasing of G_m and G_b values.

During numerical calculations, we kept $E_F^{(m)}$ and $E_F^{(b)}$ in proximity of corresponding CB edges to stay within the limits of degenerate electron gas approximation (so that (7) and (8) are valid). For lower doping levels, other expressions should be used instead of (7) and (8).

3.4. G-doping for high electron mobility applications

Realization of G-doping is attractive from the point of view of high mobility applications. Let us use a multi junction solar cell [25] as an example to estimate G-doping improvement of its characteristics. In this device, window, emitter and tunnel junction layer doping levels are roughly 10^{18} cm^{-3}. At this level of donor doping, ionized impurities reduce electron mobility by a factor of 4 in GaAs [26] (at *T*=300 K) and by the factor of 10 in Si [27]. Most types of solar cells use transparent conductive oxides with doping levels of 10^{20}-10^{21} cm^{-3}. At this donor doping level ionized impurities reduce electron mobility by the factor of 30-50 in GaAs. Thus, using G-doping in these layers can dramatically improve characteristics of solar cells.

Multiple NG layers can be realized by epitaxial growth on the top of lead grating, previously formed on the substrate. Such structure has been modelled [28] and fabricated [29] on GaAs substrate using epitaxial growth technique. Layers, grown using this technique, have diverse geometry compared to single NG layer. They have gratings from both sides and interfaces resemble sine instead of square. With increasing number of layers sine amplitude reduces and finally one gets plain layers. Geometry factor and G-doping level reduce with increasing of layer number. It is challenging to obtain high *G* values or considerable DOS reduction in both NG and alike geometries. However, as table 1 shows, G-doping required values are quite close to unity (especially for the main layer). The obtaining of such values in multiple NG systems seems to be straightforward.

The above analysis was made using the assumption of G energy independence (3). Usually, electron confinement energy regions are small (tens or hundreds of meV) and this assumption is valid. However, the NG layer can be made free standing or grown on very wide band gap substrate. In these cases, confinement energy intervals are much wider and care should be taken when assuming G energy independence.

4. Thermoelectric properties of nanograting layers

Thermoelectric materials are characterized in terms of the dimensionless figure of merit *ZT*. Here, *T* is the temperature and *Z* is given by $Z = \sigma S^2 / (\kappa_e + \kappa_l)$, where S is the Seebeck coefficient, σ is electrical conductivity, κ_e is an electron gas thermal conductivity, and κ_l is lattice thermal conductivity. The difficulty in increasing *ZT* is that materials having high S usually have low σ. When σ is increased, it leads to an increase in κ_e, following Wiedemann–Franz law, and *ZT* does not

improve much. Another approach is to eliminate the lattice thermal conductivity by introducing vacuum nanogap between the hot and cold electrodes [30–32] and using electron tunnelling. Cooling in such designs was observed in [33] and theoretically studied in [34]. However, vacuum nanogap devices appear extremely difficult to fabricate. In this work, we present a solution that allows large enhancement of S without changes in σ, κ_e, and κ_l. It is based on having a series of p–n junctions on the top of the NG.

It is another objective of this work is to calculate ZT of NG with series of p–n junctions and compare it with Z_0T of reference nanograting (RNG), in which $G \neq G(T)$, and bulk material. The reduced figure of merit ZT / Z_0T is calculated and μ dependences are presented for such traditional thermoelectric materials as Si and Ge. Analysis was made within the parabolic bands approximation and the abrupt junction's approximation. Since only heavy G-doping was considered, we neglected the hole contribution in transport.

4.1 Charge and heat transport in the NG layer with p-n junctions

Here, we propose a system composed of NG layer and an additional layer on the top of the ridges forming periodic series of p+–n+ junctions (Figure 5). In such system, charge depletion region

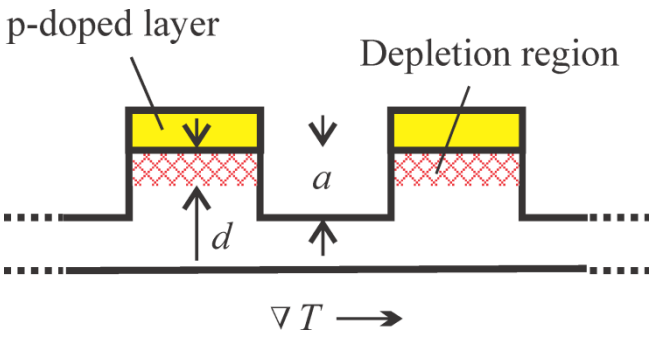

Figure 5. NG with series of periodic junctions grown at the top of the ridges.

develops inside the ridges and effective ridge height reduces, becoming a rather strong function of temperature T. Consequently, T-dependence of chemical potential μ magnifies and Seebeck coefficient S increases. Depletion region width $d(T)$ depends rather strongly on temperature. The ridge effective height $a_{\text{eff}}(T) = a - d(T)$ and consequently the geometry factor G becomes temperature-dependent, $G = G(T)$. All parameters of NG layer including μ become stronger functions of T than it will be in an NG layer without the junctions. Seebeck coefficient and thermoelectric figure of merit increase.

Analysis was made using the Boltzmann transport equations. First, we calculate $\nabla\mu$ for the system of NG layer and junctions and express it as

$$\nabla\mu = \nabla\mu_0 + \nabla\mu_J \qquad (11)$$

Here, $\nabla\mu_0$ is the chemical potential gradient in an RNG (NG layer without p-n junctions) and $\nabla\mu_J$ is introduced by the junctions. Next, we insert $\nabla\mu$ in Boltzmann transport equations and calculate S for the system of NG layer and junctions, expressing it as $S = S_0 + S_J$, where S_0 is Seebeck coefficient of RNG and S_J is introduced by the junctions.

Cross-section of the system of NG and periodic junction is shown in figure 5. We assume that there is a temperature gradient ∇T in the Y-dimension. Consequently, depletion depth depends on the Y-coordinate, and geometry factor gradient ∇G appears in the Y-direction. The presence of ∇G and ∇T modifies the electron distribution function and causes electron motion from the hot side to the cold side. This motion is compensated by thermoelectric voltage. Let us write Boltzmann transport equations [35] for the system of NG layer and periodic series of junctions

$$J = \mathbf{L}^{11}\left(\mathcal{E} + \nabla\mu / e\right) - \mathbf{L}^{12}\nabla T \text{ and } J^{Q} = \mathbf{L}^{21}\left(\mathcal{E} + \nabla\mu / e\right) - \mathbf{L}^{22}\nabla T \qquad (12)$$

Here, J is the electric current density, J^{Q} is the heat current density, $\mathbf{L}^{ij}$ are coefficients, $\mathcal{E}$ is the electric field, and e is the electron charge. Within the parabolic band approximation, $\mathbf{L}^{ij}$ are the functions of integrals of type [36].

$$\Omega^{(\alpha)}(E) = \int_{-\infty}^{+\infty} dE\left(-\partial f_0 / \partial E\right)\rho(E)\tau(E)\mathrm{v_y}^2 (E-\mu)^{\alpha} \qquad (13)$$

where f_0 is the electron distribution function, $\tau(E)$ is the electron lifetime, $\mathrm{v_y}$ is the electron velocity in the Y-direction, and α = 0, 1, 2. Let us find how NG affects $\Omega^{(\alpha)}(E)$. The NG does not change dispersion relation and consequently $\mathrm{v_y}$. It reduces density of states (3D density) G times, i.e. $\rho(E) = \rho_0(E)/G$ and increases the transport lifetime G times [21], i.e., $\tau(E) = G\tau_0(E)$ (the later follows from Fermi's golden rule). Here, $\rho_0(E)$ and $\tau_0(E)$ are the density of states and carrier lifetime, respectively, in the case a = 0. Consequently, product $\rho(E)\tau(E)\mathrm{v_y}^2$ in the NG layer is the same as in the conventional wide quantum well of the same width (3D case) and in the bulk material. This product does not depend on G and consequently it becomes independent of depletion depth. The NG changes the distribution function f_0, since it increases μ. The NG influences integrals $\Omega^{(\alpha)}(E)$ by changing μ alone. Therefore, the integrals are the same as in the bulk material having the corresponding chemical potential

$$\mathbf{L}^{ij} = \mathbf{L}_0{}^{ij}. \qquad (14)$$

where $\mathbf{L}_0{}^{ij}$ are the coefficients of bulk material having the value of μ obtained by the conventional doping (for instance).

Further, we have to find μ for the system of NG layer and junctions and insert it in (12) together with (14). The chemical potential of degenerated semiconductor ($-2 < \mu^* < 2$ where $\mu^* = \mu / k_{\mathrm{B}}T$) can be written as [37] (note that frequently Fermi energy is used instead of chemical potential in semiconductor literature)

$$\mu = k_{\mathrm{B}}T\left[\ln\left(n / N_{\mathrm{NG}}\right) + 2^{-3/2}\left(n / N_{\mathrm{NG}}\right)\right] \qquad (15)$$

where n is the electron concentration and N_{NG} is the effective conduction band density of states of NG layer. In the case of heavy G-doping ($n >> n_{\mathrm{i}}$, where n_{i} is intrinsic concentration), we can use (3)

for *n*. Density of states reduces *G* times in NG layer, i.e. $N_{\mathrm{NG}} = N_{\mathrm{C}} / G$, where N_{C} is the CB effective density of states for bulk semiconductor. Inserting this and (3) in (15), we get

$$\mu = k_{\mathrm{B}} T \left\langle \ln\left[n_{\mathrm{con}} (G-1) / N_{\mathrm{C}} \right] + 2^{-3/2} \left[n_{\mathrm{con}} (G-1) / N_{\mathrm{C}} \right] \right\rangle \qquad (16)$$

Further, we rewrite (16) as

$$\mu = \mu_0 + k_{\mathrm{B}} T \left\langle \ln\left[(G-1) / (G_0 - 1) \right] + 2^{-3/2} \left(G - G_0 \right) n_{\mathrm{con}} / N_{\mathrm{C}} \right\rangle \qquad (17)$$

where G_0 is constant. Introduction of $\mu_0 \equiv \mu(G_0)$ defines reference material as n+-type semiconductor with electron concentration of $N_{\mathrm{D}} = n_{\mathrm{CON}}(G-1)$, or RNG layer having constant geometry factor $(\partial G / \partial T) = 0$ and $G = G_0$. Next, we calculate the gradient of (10) taking into account that $N_{\mathrm{C}} \propto T^{3/2}$. The result is

$$\nabla \mu = \nabla \mu_0 + \theta \nabla T \qquad (18)$$

$$\text{where } \theta \equiv k_B \left[\ln \frac{G-1}{G_0 - 1} - \frac{1}{2} \xi \left(G - G_0 \right) + T \left(\frac{1}{G-1} + \xi \right) \frac{\partial G}{\partial T} \right] \qquad (19)$$

and $\xi \equiv 2^{-3/2} n_{\mathrm{con}} / N_{\mathrm{C}}$. Inserting (18) and (14) in Boltzmann equations, we find charge and heat currents in the system of NG layer + Junctions

$$J = \mathbf{L}_0^{11} \left(\mathcal{E} + \nabla \mu_0 / e \right) - \left(\mathbf{L}_0^{12} - \mathbf{L}_0^{11} \theta / e \right) \nabla T \text{ and} \qquad (20a)$$

$$J^Q = \mathbf{L}_0^{21} \left(\mathcal{E} + \nabla \mu_0 / e \right) - \left(\mathbf{L}_0^{22} - \mathbf{L}_0^{21} \theta / e \right) \nabla T . \qquad (20b)$$

Further, Seebeck coefficient, electrical conductivity, and electron gas heat conductivity can be found from (20a) and (20b) in a conventional way.

$$S = \left(\mathbf{L}_0^{12} - \mathbf{L}_0^{11} \theta / e \right) \Big/ \mathbf{L}_0^{11} = S_0 - \left(\theta / e \right) \qquad (21)$$

$$\kappa_e = \mathbf{L}_0^{22} - \mathbf{L}_0^{21} (\theta / e) - \left(\mathbf{L}_0^{12} - \mathbf{L}_0^{11} \theta / e \right) \mathbf{L}_0^{21} \Big/ \mathbf{L}_0^{11} = \kappa_{e0} \qquad (22)$$

$$\sigma = \mathbf{L}_0^{11} = \sigma_0 \qquad (23)$$

Electrical and thermal conductivity in the system of NG layer and junctions remain unaffected (with respect to RNG layer or bulk material having the same μ value) by a series of junctions, and S change according to (21). To calculate θ and then S, we have to find $\partial G / \partial T$ first (19).

Such performance of transport coefficients has following physical interpretation. The geometry factor G is a rather strong function of temperature. Consequently, T-dependence of chemical potential magnifies and Seebeck coefficient, having approximate value $S \approx -(1/e)(\partial\mu/\partial T)$, increases. Electrical conductivity $\sigma = \Omega^{(0)}$ is G independent since, the reduction of state density leads to a proportional increase of lifetime, according to Fermi's golden rule (resulting in (14)). In a degenerate electron gas (n+-type semiconductor) Wiedemann–Franz law works well. Thus, the thermal conductivity κ_e follows σ and is also G independent.

4.2. Seebeck coefficient of NG layer with p–n junctions

It is reasonable to calculate the Seebeck coefficient of the NG layer with junctions relative to RNG layer, in which geometry factor is constant $(\partial G/\partial T) = 0$. This will allow comparison of dimensionless figure of merit *ZT* with Z_0T, using similarity of electric (23) and heat conductivities (22). In (17)–(19) G_0 is arbitrary. To simplify the comparison, we choose G_0 so that NG layer with junctions and reference RNG layer have the same μ value. Equation of chemical potentials leads to $G_0 = G$ (16). Inserting this in (19) and further inserting the obtained result in (21), we obtain for the Seebeck coefficient of the NG layer with junctions

$$S = S_0 - \frac{k_B T}{e}\left(\frac{1}{G-1} + \xi\right)\left(\frac{\partial G}{\partial T}\right) \qquad (24)$$

3D Seebeck coefficient of reference RNL does not differ from the Seebeck coefficient of the bulk material, and within the parabolic band approximation it is equal to [38]

$$S_0 = \frac{k_B}{e}\left[\frac{r+5/2}{r+3/2}\frac{\mathrm{F}_{r+3/2}(\mu^*)}{\mathrm{F}_{r+1/2}(\mu^*)} - \mu^*\right] \qquad (25)$$

Here, r refers to scattering parameter and it is assumed that electron lifetime $\tau(E) \propto E^r$, $\mu^* = \mu/k_B T$ is the reduced chemical potential, and $\mathrm{F}(\mu^*)$ are Fermi integrals. In the case of no impurities (G-doping) and low energies, acoustic phonons are responsible for electron scattering and $r = 0$. It should be noted here that NG layer has G times more width [21] with respect to the conventional layer. As 3D $\rho(E)$ in wide quantum wells tends to $\rho(E)$ of the bulk material of the same width, using (28) for RNG is a good approximation. However, in the case of thin layers oscillatory behaviour of transport coefficients should be considered [39].

To find the ratio Z/Z_0, we use relations (22) and (23) and obvious relation between lattice thermal conductivities $\kappa_l = \kappa_{l0}$, all together leading to

$$Z/Z_0 = \left(S/S_0\right)^2 \qquad (26)$$

Figure 6 shows the dependence $S_0(\mu)$ according to (25). The $S(\mu)$ in the same figure is determined by first, calculating S (G) by inserting $\partial G/\partial T$ (which was calculated in [5]) in (24), and then (16)

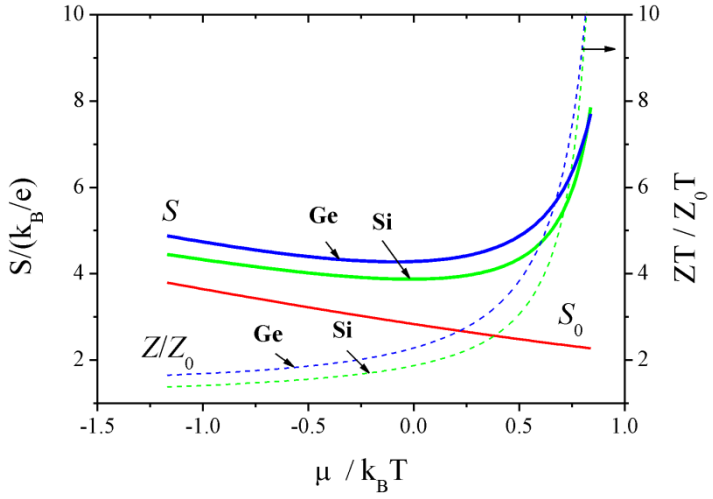

Figure 6. $S(\mu)$ – solid lines, $S_0(\mu)$ – dotted line, and $Z(\mu)/Z_0(\mu)$ – dashed lines (belong to right Y-axis). Dependences $S(\mu)$ and $Z(\mu)/Z_0(\mu)$ are calculated for Si and Ge materials.

was used to convert X-axis so that $S(\mu)$ was obtained from $S(G)$. The ratio $Z(\mu)/Z_0(\mu)$ in the same figure is calculated according to (26). We present μ dependences as they allow the understanding of possible μ ranges, within which real devices can operate without changing the sign of $(\partial G/\partial T)$ (see reference 5) and consequently S sign. Traditional thermoelectric materials Si and Ge are chosen as examples. Dependences are plotted for the following parameters: Material Si, n_{CON} = 4.5×10^{18} cm^{-3}, a = 20 nm, $\gamma = 3.3$ (γ is reduced chemical potential of p-type layer), $\beta = 0.1$ ($\beta = a_{eff}/d$), T = 300 K; Material Ge, n_{CON} = 1.4×10^{18} cm^{-3}, a = 35 nm, $\gamma = -1$, $\beta = 0.25$, T = 300 K. For both Si and Ge, we choose n_{CON} so that, for value G=10, μ was close to the optimum value $\mu_{OPT}/k_BT = r + 1/2$ [38]. It should be noted here that NG layer exhibits quantum properties at G times more widths with respect to the conventional quantum well.

Figure 6 shows large enhancement of figure of merit in p+–n+ junction NG layer both for Si and Ge materials. The dependences are quite identical for materials having rather different band gaps (1.12 eV for Si and 0.66 eV for Ge). This shows that despite the band gap value entering expressions for depletion depth (Reference 5) and $(\partial G/\partial T)$, almost similar $S(\mu)$ and $Z(\mu)/Z_0(\mu)$ dependencies can be obtained by matching such parameters as β and γ.

5. Metal nanograting layers

In the case of metal layers, electrons rejected from forbidden quantum states below Fermi energy, occupy quantum states above Fermi energy. Fermi energy moves up on energy scale and work function reduces.

Low work function (WF) electrodes [40] are essential for cold emission and room temperature operation of thermionic [41, 42] and thermotunnel [43-45] energy converters and coolers. Such devices consist of plain emitter and collector electrodes, separated by the thin vacuum gap. Electrons absorb heat energy inside the emitter electrode, overcome the vacuum barrier (or tunnel through it) and release heat energy inside the collector electrode. Electrodes require materials with work function $e\phi = 0.2 - 0.4$ eV (here, e is electron charge and ϕ potential). For most metals $e\phi$>4 eV, and only

some compounds show $e\phi$=2-3 eV. This is one order of magnitude higher than required. WF values of about 1 eV were obtained in sophisticated systems like Mo-Cs and Ag-O-Cs. However, these types of electrodes have a short lifetime even in good vacuum conditions. To overcome difficulties, quantum mechanical tunnelling was utilized. Tunnelling through vacuum nanogap allows sufficiently large currents from the electrodes, having relatively high $e\phi$ values. It was found that image force reduces the potential barrier and increases tunnelling current, giving a cooling power of 100 W/cm^2 for $e\phi \approx 1$eV [43] in mixed thermotunnel and thermionic regime. Electrons were filtered by collector coating, to increase the cooling coefficient [44] and confor mal electrode growth technology was developed [45]. However, the vacuum nanogap device appears extremely difficult to fabricate as it requires an electrode spacing of 5-10 nm. Earlier, WF reduction in Au, Nb and Cr metal NG layers was observed experimentally [46]. If an $e\phi$<1eV electrode could be obtained, poor thermionic regime can be realized at increased electrode spacing. Fabrication of wide vacuum gap, using conformal electrode technology, is much more straightforward. Low WF energy converters are essential for heat to electricity direct conversion in the temperature range 400-1000 K in which waste heat is available from the combustion sources. Low WF coolers are essential for integrated circuit cooling and other applications where low weight and ecological purity are major requirements.

Here, we calculate $e\phi$ in the metal NG layer, grown on semiconductor and metal substrates, and find out how it depends on NG dimensions and electron confinement. In the beginning we calculate $e\phi$ values in the metal NG layer forming a Schottky barrier or ohmic contact with a semiconductor substrate. Next, we calculate $e\phi$ in the metal NG layer grown on a metal substrate. Finally, the possibility of realization of such electrodes using conventional thermionic and other materials is discussed. An analysis was made within the limits of parabolic band, wide quantum well and degenerate electron gas approximations.

5.1. Work function of metal NG layer grown on a semiconductor substrate

To maintain the uniform vacuum nanogap over the whole area, electrodes should have plane geometry and smooth surface. The simplest solution is to use semiconductor substrate as an electrode base [47] and grow a thin metal NG layer on it.

The Energy diagram of the metal film grown on n+ type semiconductor substrate is shown in Figure 7a. We begin from the case when the difference between metal initial work function $e\phi_0$ and

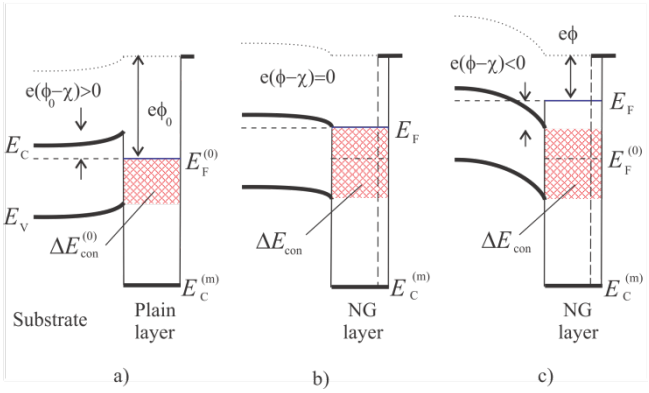

Figure 7. Energy diagram of metal-semiconductor contact in the case $e(\phi_0 - \chi) > 0$, a) without NG or G=1, b) with NG at $G = G_0$, c) with NG at $G > G_0$. Hatch depicts a confinement energy region.

semiconductor electron affinity $e\chi$ is positive, i. e. $e(\phi_0 - \chi) > 0$. We presume that electron gas in metal layer is degenerate, so that all quantum states are occupied below Fermi energy E_F and are empty above E_F. Further, suppose that the semiconductor band gap $E_g = E_C - E_V$ is wide enough, so that $e(\phi_0 - \chi) < E_g$ is satisfied. Then, electrons having energies within the region

$$\Delta E_{con}^{(0)} = E_g - e(\phi_0 - \chi) \qquad (27)$$

are confined to the metal film. Within $\Delta E_{con}^{(0)}$, quantum states for electrons are filled in the metal film and forbidden in the semiconductor substrate. Next, we fabricate ridges on the metal film surface (Fig. 7b). Additional vertical lines near the vacuum boundary in figures 7b and 7c depict extra boundary conditions, imposed by the ridges. Owing to quantum state depression, supplementary boundary conditions reduce the quantum state density G times, within the energy region $e(\chi_m - \chi) - E_g < E < e(\chi_m - \chi)$, having a width $\Delta E_{con} = E_g$. Here, we measure energies from the metal conduction band bottom $E_C^{(m)}$ and depict $e\chi_m \equiv E_F^{(0)} + e\phi_0$ as a metal conduction band width. Electrons, rejected from the forbidden quantum states within $\Delta E_{con}^{(0)}$, occupy the empty states above $E_F^{(0)}$. The Fermi level and the semiconductor band edges E_C and E_V move up on the energy scale. At the same time, $e\phi$ decreases and the energy region $\Delta E_{con} = E_g - e(\phi - \chi)$ (Eq. (5)) gets extended. As $e\phi$ decreases, the semiconductor band edge curving follows the $e(\phi - \chi)$ value and reverses its curving direction at $e(\phi - \chi) = E_C - E_F^{(0)}$.

The $e\phi$ value was calculated using electron number conservation in the NG layer conduction band. The number of electrons rejected from the forbidden quantum states was equal to the number of electrons accommodated above the initial Fermi level n_{ACC}. The rejected electron number, according to Eq. (3) was

$$n_r = (1-1/G)\int_{con} dE\,\rho_0(E) = (1-1/G)\int_{e(\chi_m-\chi)-E_g}^{e(\chi_m-\varphi_0)} dE\,\rho_0(E). \qquad (28)$$

In Eq. (28), we take into account that electrons were rejected from the energy interval $e(\chi_m - \chi) - E_g < E < e(\chi_m - \phi_0)$. They were accommodated in the interval $E_F^{(0)} < E < E_F$ or $e(\chi_m - \phi_0) < E < e(\chi_m - \phi)$. If n_r was low, the last interval fit within the ΔE_{con} (Fig. 7b) where the density of states is reduced Eq. (1). The accommodate electron number was equal to the number of empty quantum states between $E_F^{(0)}$ and E_F

$$n_{INS} = \int_{E_F^{(0)}}^{E_F} dE\,\rho(E) = \int_{e(\chi_m-\varphi_0)}^{e(\chi_m-\varphi)} dE\,\rho(E) = (1/G)\times\int_{e(\chi_m-\phi_0)}^{e(\chi_m-\phi)} dE\,\rho_0(E) \qquad (29)$$

Using condition $n_r = n_{ACC}$ and putting in $\rho_0(E) \propto E^{1/2}$, which is true within the limit of parabolic band approximation, we found after integration and simplification that

$$\underset{e\phi \geq e\chi}{e\phi} = e\chi_{\mathrm{m}} - e\left[G\left(\chi_{\mathrm{m}} - \phi_0\right)^{3/2} - (G-1)\left(\chi_{\mathrm{m}} - \chi - E_{\mathrm{g}}/e\right)^{3/2}\right]^{2/3} \tag{30}$$

Here, we use 3D density of states $\rho_0(E) \propto E^{1/2}$ (wide quantum well). Further, if n_{REJ} was high enough, $e(\phi - \chi)$ changed sign as shown in figure 7c. Here, n_{r} was calculated using Eq. (28) again. However, in this case, electrons were accommodated in quantum states from two different energy intervals. The primary interval $e(\chi_{\mathrm{m}} - \phi_0) < E < e(\chi_{\mathrm{m}} - \chi)$ was above $E_{\mathrm{F}}^{(0)}$ and within the energy region ΔE_{con} where the DOS was reduced, and the secondary interval $e(\chi_{\mathrm{m}} - \chi) < E < e(\chi_{\mathrm{m}} - \phi)$ was above $E_{\mathrm{F}}^{(0)}$ and out of ΔE_{con}. The two intervals differ by the DOS. The DOS was equal to Eq. (1) in the primary interval and $\rho_0(E)$ in the secondary one. Consequently, n_{ACC} was

$$\int_{E_{\mathrm{F}}^{(0)}}^{E_{\mathrm{F}}} dE\,\rho(E) = \int_{e(\chi_m - \phi_0)}^{e(\chi_m - \phi)} dE\,\rho(E) = (1/G)\int_{e(\chi_m - \phi_0)}^{e(\chi_m - \chi)} dE\,\rho_0(E) + \int_{e(\chi_m - \chi)}^{e(\chi_m - \phi)} dE\,\rho_0(E) \tag{31}$$

Further, equalizing Eq. (28) and Eq. (31) and repeating the above described steps we found

$$\underset{e\phi < e\chi}{e\phi} = e\chi_{\mathrm{m}} - e\left\langle\left(\chi_{\mathrm{m}} - \phi_0\right)^{3/2} + \left(1 - G^{-1}\right)\left[\left(\chi_{\mathrm{m}} - \chi\right)^{3/2} - \left(\chi_m - \chi - E_{\mathrm{g}}/e\right)^{3/2}\right]\right\rangle^{2/3} \tag{32}$$

Next, we consider the case when the difference between $e\phi_0$ and $e\chi$ was negative, i.e, $e(\phi_0 - \chi) < 0$ from the beginning (Fig. 7a). Here, $\Delta E_{\mathrm{con}}^{(0)} = E_{\mathrm{g}}$. When ridges were fabricated (Fig. 3b), the rejected electrons reduced $e\phi$. As $e\phi$ reduced $e(\phi - \chi)$ also reduced and got even more negative. Semiconductor bands curve in the direction of $E_{\mathrm{C}}^{(\mathrm{m})}$. At the same time, ΔE_{con} remains constant. Electrons were rejected from the interval $e(\chi_{\mathrm{m}} - \chi) - E_{\mathrm{g}} < E < e(\chi_{\mathrm{m}} - \chi)$, and their number was calculated by applying this interval to Eq. (4). Electrons were accommodated in the interval $e(\chi_{\mathrm{m}} - \phi_0) < E < e(\chi_{\mathrm{m}} - \phi)$ and their number was

$$\int_{e(\chi_m - \phi_0)}^{e(\chi_m - \phi)} dE\,\rho_0(E). \tag{33}$$

Using $n_{\mathrm{r}} = n_{\mathrm{ACC}}$, and repeating the above steps, we found that Eq. (32) is true for the case $e(\phi_0 - \chi) < 0$ as well.

Finally, Eq. (32) allows the calculation of geometry factor value G_0, at which an ideal ohmic contact was obtained or $e(\phi - \chi) = 0$. Inserting this in Eq. (8), we found

$$G_0 = \left[\left(\chi_{\mathrm{m}} - \chi\right)^{3/2} - \left(\chi_m - \chi - E_{\mathrm{g}}/e\right)^{3/2}\right]\left[\left(\chi_{\mathrm{m}} - \phi_0\right)^{3/2} - \left(\chi_m - \chi - E_{\mathrm{g}}/e\right)^{3/2}\right]^{-1} \tag{34}$$

Analysis of the metal NG layer/semiconductor contact shows that in the case $e(\phi_0 - \chi) \geq 0$, metal NG layer $e\phi$ was calculated using Eq. (30) if $G \leq G_0$ (or $e\phi \geq e\chi$) and Eq. (32) if $G > G_0$ (or $e\phi < e\chi$).

For the opposite case, $e(\phi_0 - \chi) < 0$, $e\phi$ was calculated using Eq. (32) for all G values (note that G>1 by definition).

6. Material pairs for nanograting layer coated electrode

The thickness of a conventional metal quantum well is only 1-5 nm [48]. NG fabrication on such thin layer surface seems complicated. However, owing to reduced quantum state density, metal NG layer retains quantum properties at *G* times more thickness (as found in Ref. 21) with respect to a conventional metal quantum well. This makes NG fabrication straightforward. In some cases, the layer thickness can be increased even more than *G* times. As figure 7 shows, confined electrons have energies $E < E_{\mathrm{F}}^{(0)} - K_{\mathrm{B}}T$ (here, K_{B} is Boltzmann constant and $K_{\mathrm{B}}T \approx 25$ meV << $E_{\mathrm{F}}^{(0)}$ for *T*=300K). For these energies, Fermi-Dirac distribution function $f(E, E_F, T) \approx 1$. Consequently, electron scattering on phonons and lattice defects is limited. Such scattering requires the exchange of a small portion of energy with the environment, which is quantum mechanically restricted as all nearby quantum states are occupied. The mean free path of such electrons is very large and is limited only by structural defects, such as grain boundaries. In epitaxial films, such electrons allow phase coherence at large distances (in transverse direction) and metal NG thickness can be increased. In this work, we do not concentrate on thermal processes in the metal NG layer by following reasons. Transport coefficients in the NG have the same values as in a conventional NG layer (having the same value of E_F) [5]. In vacuum device, the temperature gradient is applied mainly to the vacuum gap and only significant thermal process inside the electrode is Joule heating [49]. Such heating inside the metal NG layer is negligible. We regard only n+ semiconductor substrates in which, the difference $E_{\mathrm{C}} - E_{\mathrm{F}}$ is low and, heat absorption or release at the metal/semiconductor interface is insignificant.

Regular semiconductor materials can be used as base substrate. Thermionic and thermotunnel converters are high current low voltage devices. Consequently, the main limitation is electrical conductivity. Equations (30) and (32) show that the wide band gap material allows more reduction in $e\phi$. Unfortunately, it is problematic to achieve low resistivity in such materials. The most promising seems GaN in which relatively low resistivity was obtained. Other possible substrate materials are GaAs and Si. Table 2 shows possible donor concentrations N_{D} for GaN [50] , Si, GaAs [23] and corresponding

Table 2. Parameters of electrode base materials. The P_{d} and ∇T are given for 1 mm thick substrate

Substrate material	E_g (eV)	$e\chi$ (eV)	N_{D} (cm^{-3})	r (Ω cm)	P_{d} (mW) at 10 Acm^{-2}	κ ($\mathrm{Wcm}^{-1}\mathrm{K}^{-1}$)	∇T (K) at 10 Wcm^{-2}
Si	1.12	4.05	$8\ 10^{20}$	$2\ 10^{-4}$	2	1.6	0.6
GaAs	1.42	4.07	$8\ 10^{19}$	$1\ 10^{-4}$	1	0.5	2.0
GaN	3.20	4.10	$1\ 10^{19}$	$7\ 10^{-3}$	70	5.0	0.2
Mo				$5.3\ 10^{-6}$	$5.3\ 10^{-2}$	1.4	0.7
Ni				$6.2\ 10^{-6}$	$6.2\ 10^{-2}$	0.9	1.1

electrical resistivity r and heat conductivity κ. Metals, Ni and Mo, are also included since they are frequently used in thermionic converters. Table 2 also shows the dissipated power per cm^2 area P_{d}, and temperature gradient ∇T over 1 mm thick substrate, calculated for typical current density (10 $\mathrm{A/cm}^2$) and heat flux (10 $\mathrm{W/cm}^2$). Power dissipation in GaN substrate is considerable (note that ∇T is low for GaN). On the other hand, GaN has a wide band gap and allows lower $e\phi$ values. A possible solution is to grow thin GaN epitaxial layer on the GaAs or Si substrates. Such bi-layer substrate ensures low

power loss together with low $e\phi$ in the metal NG layer. Fortunately, GaN can be grown epitaxially on both GaAs and Si substrates [51].

Most technological metals have $e\phi_0 > 4$ eV and form Shottky barriers with above semiconductor materials i.e. $e(\phi_0 - \chi) > 0$. Table 3 shows the parameters of some metals frequently used as electrode materials (other interesting metals are included as well), collected from the literature: $e\phi_0$ from Ref. 52 and $E_F^{(0)}$ from Ref. 53.

Table 3. Characteristic energies for some metals and values of $e\phi$, calculated for G=10

NG Material	$e\phi_0$ [eV]	$E_F^{(0)}$ [eV]	E_F^{Band} [eV]	$e\phi$ (eV) on Si	GaAs	GaN
La B_6	2-3.2		10.0[54]	1.15	0.95	0
Ag	4.26	5.48	7.5[54]	3.32	3.10	2.02
Nb	4.30	5.32	5.5[55]	3.36	3.14	2.06
W	4.55		6.7[56]	3.58	3.34	2.14
Cu	4.65	7.0	9.1[54]	3.65	3.43	2.20
Mo	4.60		5.0[58]	3.63	3.41	2.32

It also contains data on E_F^{Band}, which is the Fermi energy obtained from *ab initio* calculations and experiments [56- 61]. Parameter E_F^{Band} differs more or less from $E_F^{(0)}$. We used E_F^{Band} instead of $E_F^{(0)}$ for Mo, W, Ni and Pt since no $E_F^{(0)}$ data was found. This substitution is acceptable as far as a parabolic band is good approximation for these metals. The $e\phi$ values presented in the table were calculated using Eq. (32). WF values were reduced by ≈ 1 eV on Si, by ≈ 1.2 eV on GaAs and by ≈ 2.3 eV on GaN substrates. Reduction is limited by the ΔE_{con} scale. The last can only be increased by increasing band gap. However, wide band gap substrates have high resistivity and were not acceptable for thermotunnel and thermionic devices. Obviously 1-2.3 eV reduction in $e\phi$ was not enough for cold emission, but it was still interesting since the plain Mo and Ni electrodes, coated with an ultra thin layer of Cs atoms, show very low WF (1-1.5 eV). WF reduction by less than mono layer of Cs atoms is a surface effect. At the same time, quantum state depression is not a surface effect. Most probably, the two mechanisms of WF reduction will sum up and result in an $e\phi$ considerably less than 1 eV. The same is true for Ag-Ba and W-Li electrodes.

Borides have $e\phi_0 < 4$ eV and for them $e(\phi_0 - \chi) < 0$ (Fig. 7). The most frequently used is Lanthanum hexaboride LaB_6, which shows $e\phi$=2-3.2 eV. Fermi energy for LaB_6 is E_F^{Band}=10 eV [54]. Inserting these values in Eq. (32) gave $e\phi$ = 0-0.85 eV for ridged LaB_6 layer on GaN substrate, $e\phi$ = 0.94-2.05 eV on GaAs substrate and $e\phi$ = 1.15-2.28 eV on Si substrate (G = 10 was used in all cases). These values were low enough for thermotunnel and thermionic devices operating at room temperatures.

Geometry factors, at which ideal ohmic contact was obtained, were calculated using Eq. (34). They were in the range $G_0 = 1 - 5$ for most material pairs. Such G_0 can easily be obtained in practice. Exceptions were Ni/Si (G_0 = 59) and Au/Si (G_0 = 16) pairs.

7. Experimental investigation of metal nanograting layers

Thin gold films, having NG on both sides, were prepared to observe the WF reduction (Figure 8). Gold was the material of choice because it does not form a natural oxide on the surface and allows

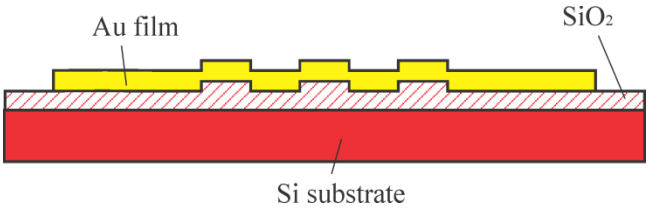

Figure 8. Cross section of Au film grown on Si substrate.

exposure of the films to the atmosphere. Au film was vacuum deposited on a Si/SiO_2 (dry thermal oxide) substrate in which NG was fabricated using both e-beam lithography and photolithography. Au was grown on a variable temperature NG substrate (T=80-300 K) using the quench deposition technique. Previously, the substrate was cooled to temperatures between -16 C and -22 C, and a thin film of 2-3 nm thickness, evaporated from a mixture of Au and Cr, was deposited on SiO2 to form an adhesive layer (not shown on figure 8 for simplicity). Following the deposition, the wafer was moved rapidly (maximum 5 s) to another location, where an Au film of thickness of 60 nm was deposited using the rapid thermal evaporation of Au wire (99.999% purity). In other cases NG in Au was made only on the surface of the film using etching techniques, while film base remained plain. Finally, large structures such as NG and plain circles and chess desk like areas containing both NG and plain squares were fabricated using photolithography.

Measurements of the work function were made using Kelvin Probe (KP) method and Photo Electron Emission Microscope (PEMM). All measurements were comparative to exclude absolute inaccuracies: KP reading from the NG area was compared to the reading from the plane area of the film. PEEM images were collected using high-resolution photoelectron microscope [62]. The internal structure of the films was analyzed using X-ray diffraction.

For all samples measured, the indented regions showed a reduced work function (WF) compared to the plain regions. The magnitude of reduction depended on the structure of the film and the dimensions of NG. The internal structure of the film was varied by changing substrate temperature. Amorphous films show a much higher reduction in WF than films with polycrystalline structure. For amorphous films the reduction of WF was in the range of 0.2-0.5 eV. All polycrystalline films show a WF reduction less than 0.1 eV. The reduction in WF was more pronounced for samples that were deposited in a cleaner environment (by plasma cleaning the deposition chamber prior to deposition). Residual gas pressure and composition has considerable influence on the results. One order difference in WF reduction shows that the internal structure of the film has principal importance.

It was observed that the strength of the effect depends on the depth of the indents. Amorphous Au films with thickness of 60 nm, and an indent depth of 50, 20 and 10 nm, show WF reduction of 0.16 eV, 0.25 eV and 0.56 eV respectively.

A WF reduction of 0.1 eV was observed in NG films grown on plain substrate. Low value of WF reduction could be explained by the fact that Au films were deposited on room temperature substrate. Another explanation is the difference in geometry. One of the samples was prepared so that it contained five areas each having a different surface geometry. The first area was plain and the other four areas had various indent widths of 800, 600, 400, 200 nm, but the same depth and length. Comparative measurements made between 1-2, 1-3, 1-4, 1-5 show that WF difference increases with reduction of indent width.

Reduction of WF of 0.2 eV was also observed in the indented areas of SiO_2. The measurement was made on several samples and yielded almost identical results.

PEEM measurements show that NG areas in all microscope images appeared brighter than adjacent plain areas (two of them were placed as on chess desk). Brighter areas corresponded to more electron emission from NG areas. This was in quantitative agreement with KP measurements. Unfortunately

PEEM microscope does not allow WF measurement on the base of image intensity. More information about experiments can be found in Reference 47.

8. Conclusions

Geometry-induced electron doping (G-doping) was investigated in multiple NG layers. They were composed of main and barrier layers forming a series of isotype homo junctions. Barrier layers were used to form electron confinement energy regions. Both main and barrier layers were n-type. Barrier layers were donor-doped to obtain electron confinement and induce G-doping in main layers. Such parameters as electron concentration, Fermi level and confinement region width were calculated for this system. Main layer G-doping level of 10^{17} -10^{18} cm^{-3} was obtained at barrier layer donor doping of 10^{18} -10^{20} cm^{-3} and geometry factor values G_m=1.02, $G_b = 1.1$. One order higher donor doping was required in Si with respect to GaAs to obtain the same G-doping level. For high electron mobility it was preferable to have high values of geometry factors. Electron mobility was higher in G-doped layers with respect to donor-doped layers of same doping level. G-doping opens prospects for new quasi-3D optoelectronic and thermoelectric systems. At the same time G-doping is temperature independent and can be used to extend working temperature ranges of cryogenic and power electronics.

Thermoelectric transport coefficients were investigated in the system of NG layers and periodic series of p–n junctions at the top of the ridges. An analysis was made on the basis of Boltzmann transport equations. It was shown that the Seebeck coefficient increases considerably. At the same time, electrical and thermal conductivities remain unaffected by the series of junctions. This allows large enhancement of thermoelectric figure of merit. Dependence of Seebeck coefficient on the geometry factor *G* and junction parameters was investigated and the analytical expression was obtained. Seebeck coefficient changes sign for some value of *G*. Dependences of S and ZT on chemical potential were presented for p–n junction NG layers. Calculations show one order of magnitude increase in thermoelectric figure of merit with respect to the bulk material.

Low work function was obtained in the metal NG layer having a reduced quantum state density. Metal LG layers, grown on semiconductor and metal substrates, were analyzed. Electron confinement to the NG layer was essential in both cases. When using semiconductor substrate, the wide band gap material allows more electron confinement and lower values of the resulting $e\phi$. Dependence of $e\phi$ on the band gap was analyzed for a number of cases and the corresponding formulae derived.

Thin Au films, having NG on both sides, were prepared using vacuum deposition, e-beam lithography and photolithography. WF reduction was measured using Kelvin Probe and verified using PEEM microscopy. Film internal structure was monitored using X-ray structural analysis. WF reduction dependence on film internal structure and NG dimensions were recorded. WF reduction of 0.56 eV was observed in Au NG films with amorphous internal structure.

9. Acknowledgements

Author thanks Ismat S. Shah and Juejun Hu for useful discussions. Apparatus received from EU TEMPUS project 530278-TEMPUS-1-2012-1-DE-TEMPUS-JPHES was used for preparation of this work.

10. References

[1] Andreozzi A, Lamagna L, Seguini G, Fanciulli M, Schamm-Chardon S, Castro C and M Perego M 2011 Nanotechnology 22 335303

[2] Xia G, Jeong S-J,Kim J E, Kimand B H, Koo C-M and Kim S O 2009 Nanotechnology 20 25301

[3] Paivanranta B, Langner A, Kirk E, David C and Ekinci Y 2011 Nanotechnology 22 375302

[4] Bergmann K, Danylyuk S V and Juschkin L 2009 J. Appl. Phys. 106 073309

[5] Tavkhelidze A 2009 Nanotechnology 20 405401

[6] Tavkhelidze A, 2010 J. Appl. Phys. 108 044313

[7] Kim J H, Barth M, Kuhl U, Stockmann H-J and Bird J P 2003 Phys. Rev. B 68 045315

[8] Berggren K-F,Yakimenko I I and Hakanen J 2010 New J. Phys. 12 073005

[9] Baltes H P and Hilf E R 1976 Spectra of Finite Systems (Wissenschaftsverlag, Mannheim)

[10] Eckhardt B 1988 Phys. Rep. 163 205-297

[11] Tavkhelidze A, Svanidze V and Noselidze I 2007 J. Vac. Sci. Technol. B 25 1270

[12] Emig T 2010 Casimir Forces and Geometry in Nanosystems, in Nonlinear Dynamics of Nanosystems, ed G. Radons, B. Rumpf, H. G. Schuster (Willey-VCH) p. 165

[13] Ono S, Shima H 2010 Physica E, 42 1224-1227

[14] Kartashov Y V, Szameit A, Keil R, Vysloukh V A, and Torner L 2011 Optics Letters 36 3470

[15] Gupta S and Saxena A 2011 J. Appl. Phys. 109 074316

[16] Fujita N 2004 J. Phys. Soc. Jpn. 73 3115-3120

[17] Ortix C, S. Kiravittaya S, Schmidt O G, and van den Brink J 2011 Phys. Rev. B. 84 045438

[18] Simon J, Protasenko V, Lian C, Xing H and Jena D 2010 Science 327 60-64

[19] Yu B, Zebarjadi M, Wang H, Lukas K, Wang H, Wang D, Opeil C, Dresselhaus M,Chen G, and Ren Z 2012 Nano Lett. 12, 20772082

[20] Goldsmid H J 2010 Introduction to Thermoelectricity (Springer)

[21] Tavkhelidze A and Svanidze V 2008 Int. J. Nanosci. 7 333

[22] Sanders A et al 2011 Nanotechnology 22 465703

[23] Sze S M and Ng K K 2007 Physics of Semiconductor Devices (New Jersey: Wiley-Interscience)

[24] Joyce W B and Dixon R W 1977 Appl. Phys. Lett. 31 354

[25] Kirk A P 2010 Solar Energy Materials & Solar Cells 94 2442

[26] Casey H C Jr and Panish M B 1978 Hetrostructure lasers (Academic press, New York)

[27] Bulucea C 1993 Solid-State Electron. 36 489

[28] Ohtsuka M and Suzuki A 1993 J. Appl. Phys. 73 7358

[29] Pickrell G W, Xu C F, Louderback D A, Lin H C, Fish M A, Hindi J J, Simpson M C, Guilfoyle P S, Zhang Z H and Hsieh K C 2004 J. Appl. Phys. 96 4050

[30] Despesse G and Jager T 2004 J. Appl. Phys. 96 5026

[31] Wachutka G and Gerstenmaier Y C 2006 proc. Int. Conference on Mixed Design (MIXDES Poland) p 48

[32] Goldsmid, H J 2003 in Thermoelectrics, 2003 Twenty-Second International Conference on ICT pp. 433- 438

[33] Hishinuma Y, Geballe T H, and Moyzhes B Y 2003 J. Appl. Phys. 94 4690

[34] Zeng T 2006 Appl. Phys. Lett. 88 153104

[35] Ashkroft N E and Martin N D 1976 Solid State Physics, (Saunders College Publishing, NY)

[36] Mahan J D and Sofo J O, 1996 Proc. Natl. Acad. Sci. USA 93 7436

[37] Joyce W B and Dixon R W 1977 Appl. Phys. Lett. 31 354

[38] Bhandari C M, Rowe D M 1995 *CRC Handbook of Thermoelectrics*, ed Rowe D M (CRC Press) p 43

[39] Rogacheva E I, Nashchekina O N, Grigorov S N, Us M A, Dresselhaus M D and Cronin S B 2002 Nanotechnology 13 1

[40] Yamamoto S 2006 Rep. Prog. Phys. 69 pp 181–232

[41] Wachutka G and Gerstenmaier Y. C. 2007 AIP Conf. Proc. 890 - 349

[42] Koh W S and Ang L K 2008 Nanotechnology 19 235402

[43] Hishinuma Y, Geballe T H, Moyzhes B Y and Kenny T W 2001 Appl. Phys. Lett. 78 2572

[44] Tavkhelidze A, Svanidze V. and Tsakadze L 2008 J. Vac. Sci.Technol. A 26 5

[45] Tavkhelidze A , Skhiladze G, Bibilashvili A, Tsakadze L, Jangidze L, Taliashvili Z, Cox I and Berishvili Z, Electron tunnelling through large area vacuum gap - preliminary results in *International Conference on Themoelectrics (ICT2002)* pp 435-439 (2002)

[46] Tavkhelidze A, Bibilashvili A, Jangidze L, Shimkunas A, Mauger P , Rempfer G F, Almaraz L, Dixon T and Kordesch M E 2006 J. Vac. Sci. Technol. B 24 1413

[47] Jangidze L, Tavkhelidze A, Blagidze Y and Taliashvili Z 2012 J. Electrochem. Soc., 159 D413-D417

[48] Su W B, Chang C S and Tsong T T 2010 J. Phys. D: Appl. Phys. 43 013001

[49] Hishinuma Y, Moyzhes B Y, and Geballe T H 2002 Appl. Phys. Lett. 81 4242

[50] Eiting C J, Grudowski P A and Dupuis R D 1998 Journal of Electronic Materials 27 206

[51] Yu J W, Lin H C, Feng Z C, Wang L S, Tripathy B S and Chua S J 2006 Thin Solid Films 498 108 – 112

[52] Linde D R 1991 *CRC handbook of Chemistry and Physics*, (71-st edition) p. 12-84

[53] Ashkroft N E and Martin N D 1976 *Solid State Physics* (NY: Saunders)

[54] Westover T L and Fisher T S 2008 Phys. Rev. B 77 115426

[55] Mizurani U 2001 *Electron theory of metals*, (Cambridge University Press) p. 27

[56] Lekka Ch E, Mehl, M J, Bernstein N and Papaconstantopoulos D A 2003 Phys. Rev. B 68 035422

[57] Lassner E and Schubert W-D 1999 *Tungsten: properties, chemistry, technology of the element, alloys, and chemical compounds* (Kluwer academic/plenum publishers NY)

[58] McAvoy T, Zhang J, C. Waldfried , D. N. McIlroy, P. A. Dowben, O. Zeybek, T. Bertrams, and B. S. Barrett 2000 The European Physics Journal B 14 747–755

[59] U. Mizurani, *Electr* J 2001 O*n theory of metals*, (Cambridge University Press) p. 27

[60] Yamasaki A and Fujiwara T 2003 J. Phys. Soc. Jpn. 72 607-610

[61] Baud S, Ramseyer C, Bihlmayer G, Blügel S, Barreteau C ,Desjonquères M C, Spanjaard D and Bernstein N 2004 Phys. Rev. B 70 235423

[62] Rempfer G F, Skoczylas W P, and Hayes Griffith O 1991 Ultra-Microscopy 36 196